Stage-dependent cardiac regeneration in *Xenopus* is regulated by thyroid hormone availability

Lindsey N. Marshall[a,1], Céline J. Vivien[a,b,1], Fabrice Girardot[a], Louise Péricard[a], Pierluigi Scerbo[a,c], Karima Palmier[a,d], Barbara A. Demeneix[a,2], and Laurent Coen[a,2,3]

[a]Evolution des Régulations Endocriniennes, Département Adaptation du vivant, CNRS UMR 7221, Muséum National d'Histoire Naturelle, Sorbonne Université, 75231 Paris, France; [b]Murdoch Children's Research Institute, The Royal Children's Hospital, Melbourne, VIC 3052, Australia; [c]Institut Curie, CNRS UMR 3347, INSERM U1021, Centre Universitaire, F-91405 Orsay, France; and [d]Institute for Integrative Biology of the Cell, Commissariat à l'Energie Atomique, CNRS UMR 9198, Université Paris Sud, Saclay, 91198 Gif-sur-Yvette, France

Edited by Deepak Srivastava, Gladstone Institute of Cardiovascular Disease, San Francisco, CA, and accepted by Editorial Board Member Roeland Nusse January 15, 2019 (received for review March 6, 2018)

Despite therapeutic advances, heart failure is the major cause of morbidity and mortality worldwide, but why cardiac regenerative capacity is lost in adult humans remains an enigma. Cardiac regenerative capacity widely varies across vertebrates. Zebrafish and newt hearts regenerate throughout life. In mice, this ability is lost in the first postnatal week, a period physiologically similar to thyroid hormone (TH)-regulated metamorphosis in anuran amphibians. We thus assessed heart regeneration in *Xenopus laevis* before, during, and after TH-dependent metamorphosis. We found that tadpoles display efficient cardiac regeneration, but this capacity is abrogated during the metamorphic larval-to-adult switch. Therefore, we examined the consequence of TH excess and deprivation on the efficiently regenerating tadpole heart. We found that either acute TH treatment or blocking TH production before resection significantly but differentially altered gene expression and kinetics of extracellular matrix components deposition, and negatively impacted myocardial wall closure, both resulting in an impeded regenerative process. However, neither treatment significantly influenced DNA synthesis or mitosis in cardiac tissue after amputation. Overall, our data highlight an unexplored role of TH availability in modulating the cardiac regenerative outcome, and present *X. laevis* as an alternative model to decipher the developmental switches underlying stage-dependent constraint on cardiac regeneration.

Xenopus | thyroid hormone | metamorphosis | cardiac regeneration | extracellular matrix

Heart failure kills more people than any other disease worldwide (1). The incapacity of the adult human heart to regenerate after ischemic events leads to damaged cardiac muscle, cardiomyocyte loss without significant replacement, and the formation of a noncontractile scar (2). The need for model organisms to analyze the mechanisms leading to heart failure is of major biomedical and fundamental relevance for development of future regenerative strategies, and ultimately to provide clinical therapies.

Intense research in the cardiac regenerative field focuses on developing a wide spectrum of model organisms to decipher mechanisms and factors involved in heart repair and scarring (3–5). Nonamniote vertebrates, such as urodeles or teleosts—with the exception of medaka (6)—possess robust lifelong cardiac regenerative capacity (5, 7). Conversely in mammals, cardiac lesions lead to scar formation rather than regeneration, as observed for adult humans (2), as well as adult mice (8), rats (9), sheep (10), pigs (11), and in rabbits after birth (12, 13). However, the neonatal mouse heart regenerates efficiently (8). Cardiac regeneration has also been reported for embryonic sheep, neonatal pigs, and rabbits (10–13). Remarkably, this has also been observed in a human neonate, with complete functional recovery following a severe myocardial infarction at birth (5, 14). Why species differ in their cardiac regenerative capacities and why this capacity is lost during mammalian development remain an enigma.

Currently, cardiac regeneration studies are dominated by the use of zebrafish and mice models. Remarkably, it is between these two evolutionary separated species that the capacity to regenerate the adult heart is thought to have been lost. Attempts to fill the knowledge gap between teleosts and mice have largely relied on studies in urodeles (such as newt and axolotl), while generally ignoring other amphibians, notably anurans, including *Xenopus* (5, 7). However, *Xenopus laevis* is considered a leading model for regeneration research, notably for studies relative to tail and limb regeneration (15). It is therefore surprising that cardiac regeneration has been overlooked in this established model system. We recently showed that, similar to adult mammals, cardiac regenerative capacity is absent in adult *Xenopus* frogs (16), but whether such ability is present at the larval stage remained to be explored. The role of thyroid hormone (TH) has been extensively investigated in *Xenopus*, where metamorphosis is a well-established model for dissecting the mechanisms underlying TH action. Several observations have shown that TH-regulated metamorphosis in amphibians diminishes the regenerative capacity of various tissues (15). Interestingly, metamorphosis is physiologically similar to early mammalian postnatal development, a time window concurrent with the loss of cardiac regeneration in mice. We thus took advantage of *X. laevis* as a relevant model to explore TH influence on the cardiac regenerative process.

Significance

Heart failure is the leading cause of death worldwide. Cardiac regeneration studies currently focus on zebrafish, urodeles, and mammals, bypassing the amphibian *Xenopus laevis*, despite being considered as a leading model for regeneration research. We thus took advantage of *X. laevis* as a model to explore thyroid hormone (TH) influence on the cardiac regenerative process. We suggest a possible link between altered TH availability and the loss of cardiac regenerative capacity. Examining heart regeneration in *Xenopus* provides insight into how TH levels may contribute to the enigmatic loss of cardiac regeneration during vertebrate development, suggesting potential therapeutic leads of major biomedical and fundamental relevance for the development of future regenerative strategies, and ultimately to provide therapies for the human heart.

Author contributions: L.N.M., C.J.V., B.A.D., and L.C. designed research; L.N.M., C.J.V., F.G., L.P., P.S., K.P., and L.C. performed research; L.N.M., C.J.V., F.G., L.P., B.A.D., and L.C. analyzed data; and L.N.M., C.J.V., F.G., B.A.D., and L.C. wrote the paper.

The authors declare no conflict of interest.

This article is a PNAS Direct Submission. D.S. is a guest editor invited by the Editorial Board.

[1]L.N.M. and C.J.V. contributed equally to this work.

[2]B.A.D. and L.C. contributed equally to this work.

[3]To whom correspondence should be addressed. Email: coen@mnhn.fr.

This article contains supporting information online at www.pnas.org/lookup/suppl/doi:10.1073/pnas.1803794116/-/DCSupplemental.

Published online February 12, 2019.

We investigated cardiac regeneration during postembryonic development and aging in *X. laevis*, focusing on the period around the peak of TH that orchestrates metamorphosis. We found that tadpoles possess efficient cardiac regeneration, a capacity that is reduced during TH-regulated metamorphosis and permanently lost in juvenile frogs. Using a pharmacological approach, we observed that either a short exogenous exposure to the most biologically active form of TH, triiodothyronine (T_3), or inhibiting TH action by using sodium perchlorate (goitrogenic effects of perchlorate inhibit TH production) before cardiac resection significantly, but differentially, altered gene expression and kinetics of extracellular matrix (ECM) component deposition. Both treatments negatively impacted myocardial wall closure and impeded tadpole heart regeneration. Our data correlate altered TH availability and the loss of cardiac regenerative capacity, and suggest that critical, fine-tuning of hormone availability can be involved in determining successful regeneration.

Results

Complete Ventricle Rebuilding Occurs After Amputation in Prometamorphic Tadpoles. We performed a simple surgery to injure *X. laevis* heart. Adapting the resection protocol previously used to study zebrafish cardiac regeneration (17), a mechanical amputation of ∼10–15% of the heart apex was performed on prometamorphic tadpoles [Nieuwkoop and Faber (NF) 57]. The main procedure includes anesthetizing the tadpole, then under a stereo microscope, exposing the heart by cutting the nearby abdominal skin, opening the pericardium, and amputating a fraction of the ventricle at the cardiac apex (Fig. 1, *Top*). A success rate (i.e., percentage of tadpoles surviving following surgical resection) of 80–90% is achieved and easy manipulation with high reproducibility enables this method to be used to analyze the previously undescribed outcome of cardiac resection at this stage of *Xenopus* development.

At 3 d postamputation (dpa), extensive fibrotic tissue (Fig. 1), principally constituted of fibronectin (*SI Appendix*, Figs. S1*A* and S2) and collagen (*SI Appendix*, Fig. S3 *A–E′*), was observed at the injured cardiac site. Serial histological analysis at successive days postamputation revealed a progressive disappearance of fibrotic tissue in the injured ventricle (Fig. 1 and *SI Appendix*, Figs. S2 and S3 *A–E′*). We observed increased fibrosis during the first 14 dpa (Fig. 1 *A–C′*), with intense labeling of fibrotic tissue (red staining) at 14 dpa (Fig. 1 *C* and *C′*). Concurrently, collagen was mostly detected at 3 dpa, decreasing but visible at 7 dpa, decreasing further at 14 dpa, and with complete resorption at 30 dpa (*SI Appendix*, Fig. S3 *A–E′*). From 30 dpa up to 90 dpa (Fig. 1 *D–F* and *D′–F′*), fibrotic resorption and regression was observed in most of the hearts analyzed ($n = 5$ of 7), showing complete disappearance and a full restoration of the resected myocardium (Fig. 1 *F1* and *F1′*), although a significant fraction ($n = 2$ of 7) still displayed incomplete rebuilding of the cardiac ventricle with partial fibrosis remaining at the amputation site (Fig. 1 *F2* and *F2′*). At 180 dpa, all tadpole ventricles presented a normal shape, a recovered continuous myocardial wall with a total disappearance of the fibrotic tissue at the apex (Fig. 1 *G* and *G′*). Thus, it was not possible to distinguish a previously resected heart from non-amputated controls. Hence, heart resection induced a transient fibrotic response in *Xenopus* tadpoles with complete fibrotic tissue disappearance at 180 dpa. These data suggest that, contrary to the adult frog that is unable to regenerate (16), the heart of a tadpole can fully regenerate within 6 mo postamputation (mpa).

Heart Regenerative Capacity Is Reduced During Metamorphosis. We next analyzed cardiac regenerative capacity during the metamorphic period, a development process orchestrated by TH (18). Prometamorphic (NF57–58) tadpoles and metamorphic stages (NF61–62 and NF65–66 tadpoles and froglets) were operated as described above and the regenerative capacity of the ventricle assessed on hearts collected at 6 mpa (Fig. 2*A*), a time sufficient

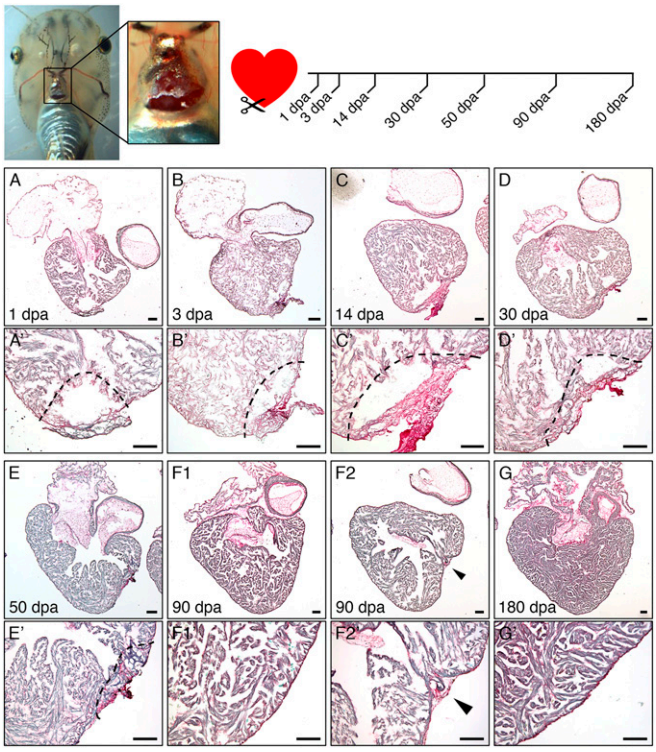

Fig. 1. Transient fibrotic response followed by complete ventricle rebuilding after cardiac resection in tadpole heart. (*Top*) Cardiac resection was performed on prometamorphic NF57 *X. laevis* tadpoles by dissecting the abdominal skin and opening the pericardium, then removing ∼10–15% of the ventricle toward the apex. Hearts were collected at 1, 3, 14, 30, 50, 90, and 180 dpa. (*A–G*) PSR histological labeling reveals an intensification of fibrotic connective tissue up to 14 dpa at the site of amputation (labeled in dark red). From 30 dpa up to 90 dpa, the fibrotic zone regressed and progressively disappeared as the ventricle apex regained a normal morphology, and was strongly reduced or undetectable after 90 (F2 and F1, respectively) or 180 dpa (*G*). (*A′–G′*) Higher magnifications, with dotted lines indicating amputated area and arrows indicating the amputation site. (Scale bars, 100 μm.)

for a complete recovery of a normal ventricle shape in NF57 tadpoles (Fig. 1). The heart grows markedly during metamorphosis and postmetamorphic development, as shown by comparing tadpole, froglet, and juvenile heart sizes, as well as when comparing the different developmental stages analyzed at 6 mpa (*SI Appendix*, Fig. S4). We noted that the extent of fibrotic connective tissue at 3 dpa in froglets is similar to that observed in tadpoles (*SI Appendix*, Fig. S1*B*). After 6 mpa, histological labeling revealed three ventricle categories displaying complete, partial, and absent regeneration (Fig. 2*B*, *Upper*, green, orange, and red boxes, respectively). In the case of absence of regeneration (i.e., presence of a permanent fibrotic scar), two morphologies were observed, both showing an invasive fibrosis in the myocardium walls that were either closed, or not, by a "fibrotic bridge" (Fig. 2*B*, *Upper*, red boxes). While all NF57–58 tadpole hearts had fully regenerated at 6 mpa (Fig. 2*B*, *Lower*) as previously observed (Fig. 1 and *SI Appendix*, Fig. S3), regeneration was incomplete for more than 45% of animals from climax to the end of metamorphosis (NF61–62 to froglet) (Fig. 2*B*). Presence of collagen in froglet hearts was still detected at 30 dpa (*SI Appendix*, Fig. S3 *F–J′*), whereas specific labeling of collagen1 (Col1) displayed a progressive but slower decrease than observed for tadpoles (*SI Appendix*, Fig. S3, compare *SI Appendix*, Fig. S3 *A′–E′* and *F′–J′*). These data indicate that cardiac regenerative capacity was impeded as metamorphosis progressed.

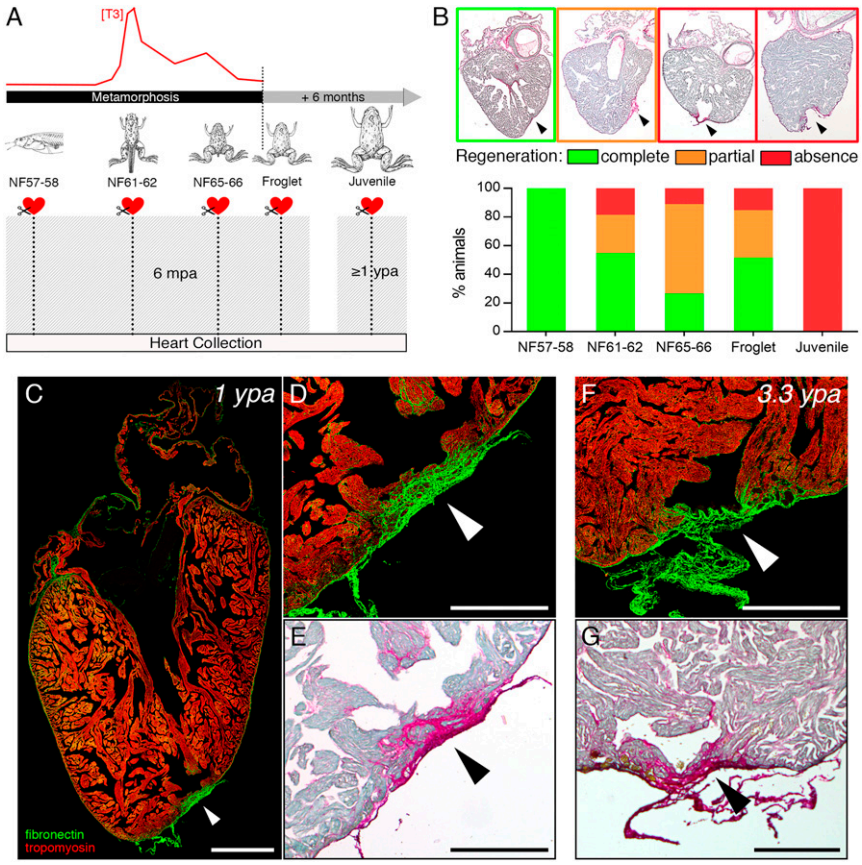

Fig. 2. Cardiac regenerative capacity is reduced then permanently lost after metamorphosis. (*A*) Cardiac resection was performed at different developmental stages before, during, and after TH-dependent metamorphosis: prometamorphic stages (NF57–58), climax (NF61–62), end (NF65–66), and just after metamorphosis (froglet), and in 6-mo-old juveniles. Hearts were collected 6 mpa for metamorphic stages (NF57 to froglet), and ≥1 ypa for juveniles. (*B*) Using PSR histological staining, hearts were categorized and quantified according to different heart phenotypes observed: fully regenerated (green: no fibrotic tissue present at the amputated site), partially regenerated (orange: fibrotic tissue remaining present at the amputated site), and those displaying an absence of regeneration (red: strong appearance of a fibrotic scar at the amputated site); arrowheads indicate the amputation site. All samples were obtained from more than four independent experiments: NF57–58, $n = 4$; NF61–62, $n = 15$; NF65–66, $n = 8$; froglet, $n = 6$, juvenile, $n = 7$. Immunolabeling (*C* and *D*) fibronectin (green), tropomyosin (red), and PSR staining (*E*) of a juvenile heart at 1 ypa ($n = 5$) displaying a clear presence of invasive fibrotic tissue at the amputation site (arrowhead). Immunolabeling (*F*) and PSR staining (*G*) of a juvenile heart at 3.3 ypa ($n = 2$) still showing a strong presence of fibrotic tissue and, hence, a persistent scar at the amputation site (arrowhead). (Scale bars, 1 mm in*C* and 0.5 mm in *D*–*G*.)

Heart Regenerative Capacity Is Permanently Lost After Metamorphosis. The ventricle of a 6-mo-old juvenile frog was larger than that of a prometamorphic tadpole (13.5-fold for the maximal area observed and 3.7-fold for the maximal perimeter) (*SI Appendix*, Fig. S4). Approximately 8% of the apex was removed by ventricular resection in frogs of this age. Regeneration was not observed after 1 y postamputation (ypa) in any frog (Fig. 2 *A* and *B* and *SI Appendix*, Fig. S3). During this postamputation time, the maximal ventricle area of the juveniles increased around threefold (*SI Appendix*, Fig. S4). A strong and invasive fibrotic and collagenous scar remained present in juvenile frogs at 1 ypa (Fig. 2 *C*–*E* and *SI Appendix*, Fig. S3 *K*–*O*). Moreover, scarring persisted at 3.3 ypa in juveniles, with hearts displaying permanent and extensive fibronectin and collagen at the apex, including a bridge of dense connective tissue (Fig. 2 *F* and *G* and *SI Appendix*, Fig. S3 *P* and *Q*). Similar results were seen in adults, where a dense collagenous scar was observable after 1 ypa (*SI Appendix*, Fig. S3 *R*–*T*). Interestingly, when we compared fibronectin labeling at the cardiac apex between a tadpole and juvenile in the first month postamputation (*SI Appendix*, Fig. S2), different dynamics of protein deposition were seen. These data indicate that cardiac regenerative capacity was completely lost after metamorphosis.

Tadpoles and Juveniles Display DNA Synthesis in Cardiomyocytes Following Heart Amputation. We investigated cardiomyocyte DNA synthesis in the injured heart of prometamorphic NF57 tadpoles that can entirely rebuild their cardiac ventricle after amputation (Figs. 1 and 2), compared with 6-mo-old juveniles, where no regeneration is observed (Fig. 2). After cardiac resection, a pulse of EdU labeling was performed for 1 wk to label all cells that undergo DNA synthesis during this time period, followed by a 1-wk chase (Fig. 3*A*). DNA synthesis in cardiomyocytes can be identified at 14 dpa as cell nuclei positive for EdU and labeled with the cardiomyocyte-specific nuclear marker myocyte enhancer factor-2 (Mef2) (Fig. 3 *B*–*C′*). This protocol was applied to nonoperated (CTRL) and sham-operated (SHAM) animals as comparative controls for amputated (AMP) animals (Fig. 3*A*).

Compared with CTRL and SHAM, AMP tadpole hearts showed a significantly higher number of EdU/Mef2 colabeled cardiomyocyte nuclei next to the amputated area (Fig. 3 *D*–*F* and *J*), whereas ventricular resection induced a slight but insignificant increase of colabeled nuclei in the rest of the ventricle (*SI Appendix*, Fig. S5 *C*–*F*). For CTRL (Fig. 3 *D* and *J* and *SI Appendix*, Fig. S5 *A* and *D*–*F*) and SHAM (Fig. 3 *E* and *J* and *SI Appendix*, Fig. S5 *B* and *D*–*F*), weak cardiomyocyte DNA synthesis was observed in the whole ventricle. Interestingly, increased cardiomyocyte DNA synthesis was also observed at the site of

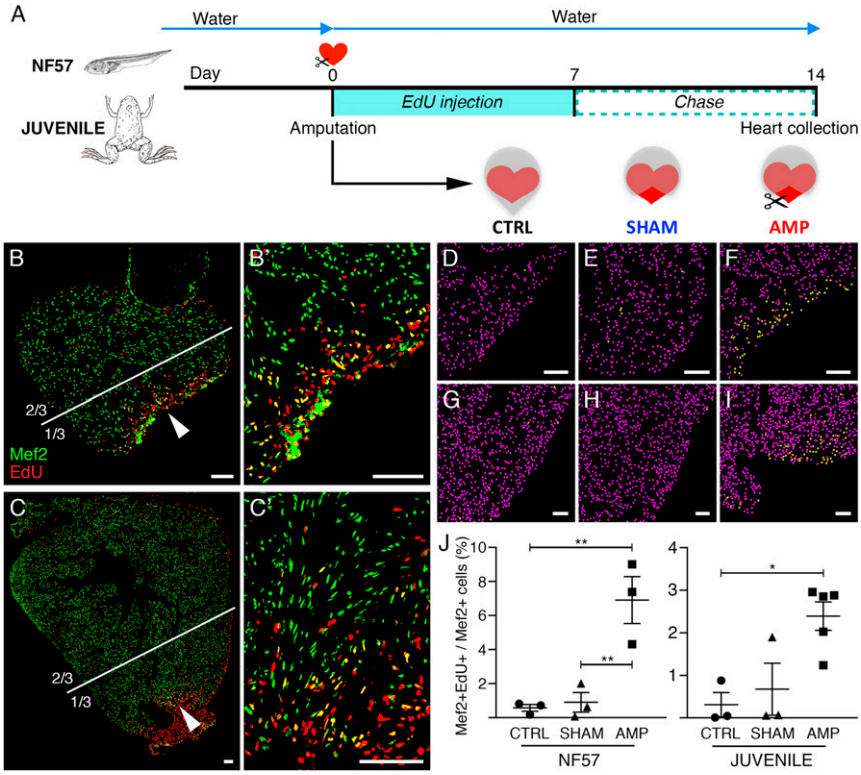

Fig. 3. Increased DNA synthesis is observed in tadpole and juvenile cardiomyocyte nuclei after heart amputation. (*A*) DNA synthesis in cardiomyocytes was assessed in amputated tadpole and juvenile hearts using EdU treatment for 1 wk (pulse), followed by a 1-wk chase period. (*B* and *C*) Immunolabeling with Mef2 antibody (green) and EdU detection (red) at 14 dpa. DNA synthesis in cardiomyocytes, characterized by colabeled $Mef2^+/EdU^+$ (yellow) nuclei, are observed in both tadpole (*B*, and magnification *B′*) and juvenile hearts (*C*, and magnification *C′*); arrowheads indicate the areas magnified in *B′* and *C′*. (*D–J*) $Mef2^+$ (converted to purple dots) and $Mef2^+/EdU^+$ (converted to yellow dots) nuclei were quantified in one-third of the ventricle at the apex for tadpoles (*D–F*) and juveniles (*G–I*): white lines define the corresponding one-third area analyzed for the tadpole (*B*) and the juvenile (JUV) (*C*) (see *SI Appendix*, Fig. S5 for remaining two-thirds quantification). Analyses were performed for nonoperated animals (CTRL, *D* and *G*), animals operated without (SHAM, *E* and *H*) and with ventricular resection (AMP, *F* and *I*). The ratio of colabeled nuclei ($Mef2^+EdU^+$) over total number of cardiomyocyte nuclei ($Mef2^+$) was calculated (*J*). All samples were obtained from two independent experiments. $n \geq 3$ for each group and ≥3 sections were quantified for each sample, and graphed, representing mean with SEM. NF57 values were normally distributed, therefore a one-way ANOVA followed by Sidak's multiple comparisons test was performed. A normal distribution was not observed for JUV; therefore a nonparametric Kruskal–Wallis test followed by a Dunn's multiple comparisons test was performed (*$P < 0.05$; **$P < 0.01$). (Scale bars, 100 μm.)

amputation in juvenile hearts, compared with CTRL and SHAM (Fig. 3 *G–J*). However, as seen for tadpoles, heart injury did not induce a significant change in cardiomyocyte DNA synthesis in the whole juvenile ventricle (*SI Appendix*, Fig. S5 *G–L*).

However, although cardiomyocyte DNA synthesis was observed at the amputated site after resection in both developmental stages, the increase was higher in tadpoles (~7%) that regenerate their heart efficiently, than in juveniles (~2.5%) that are unable to regenerate (Fig. 3*J*).

TH Excess and Deprivation Before Cardiac Resection Increase Degree of Fibrosis in Tadpoles. Because cardiac regenerative capacity is constrained during TH-controlled metamorphosis, we analyzed the consequences of a short (3 d) exposure to TH (Triiodothyronine, T_3 10^{-10} M) and of TH deprivation (perchlorate pretreated tadpoles) before cardiac amputation, on the regenerative capacity of prometamorphic NF57 tadpoles (Fig. 4*A*). The survival of T_3-treated, perchlorate-treated, and untreated tadpoles was monitored following heart amputation (Fig. 4*B*). Both exposed and unexposed animals underwent metamorphosis during this time frame. As expected, compared with untreated controls, T_3-treated tadpoles displayed an accelerated metamorphosis due to the excess TH. In contrast, in tadpoles subjected to perchlorate treatment, metamorphosis was significantly delayed by about 3 wk compared with untreated control animals. An increased death rate was observed for the T_3-treated group, but no significant difference in survival was seen for the perchlorate-treated group compared with controls. Approximately 95% of control animals survived following cardiac amputation, yet more than 50% of T_3-treated tadpoles died during the same period.

Extent of fibrosis was measured in T_3-treated and perchlorate-treated animals and compared with nontreated control animals at 30 dpa and 90 dpa (Fig. 4*C*). Absence of fibrotic tissue was observed at 90 dpa in the nontreated (CTRL) amputated group (Fig. 4*E*), as previously observed (Fig. 1), with almost complete myocardium restoration in tadpoles at 90 dpa. At 30 dpa, there was a significantly greater extent of fibrosis measured in T_3-treated animals compared with nontreated controls, whereas no significant difference was seen with perchlorate-treated animals (although we noted high variability in the group) at 30 dpa (Fig. 4*C*). Compared with 30 dpa, a decrease in fibrosis extent at 90 dpa was observed in the T_3-treated group, indicating that fibrotic regression in the injured zone also occurred in T_3-treated tadpoles. However, a significantly greater extent of fibrosis remained in T_3-treated compared with nontreated control tadpoles at this time (Fig. 4*C*). For perchlorate-treated animals, fibrosis extent at 90 dpa was still high, as if the heart was unable to regenerate. Moreover, in T_3-treated and perchlorate-treated tadpoles invasive fibrotic tissue was still present in the amputated area at 90 dpa, extending into the myocardium (Fig. 4*E*). Collagen detection confirmed these observations (*SI Appendix*, Fig. S6).

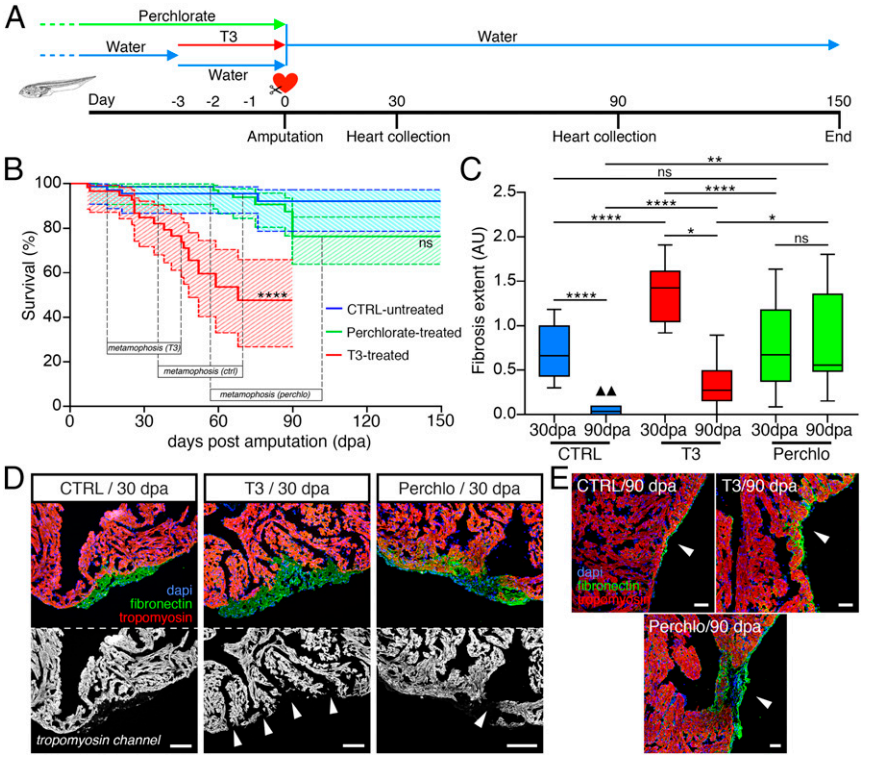

Fig. 4. Short TH exposure or deprivation before tadpole heart amputation hinders the regenerative capacity. (*A*) A ventricular resection was performed on tadpoles following a 3-d TH-pretreatment (T_3, 10^{-10} M) or treated with the goitrogen perchlorate for more than 2 mo. Hearts were analyzed at 30, 90, and 150 dpa and compared with nontreated amputated tadpoles as a control (CTRL). (*B*) Survival curves for all groups. Significantly increased mortality was observed for T_3-treated tadpoles compared with CTRL following amputation, whereas no significant difference in survival up to 150 dpa was seen with perchlorate-treated tadpoles. The time period corresponding to the metamorphosis of the experimented tadpoles are indicated. (*C*) Fibrosis extent drastically diminished between 30 and 90 dpa in CTRL, but remained significantly present for both T_3-treated and perchlorate-treated tadpoles at 90 dpa. (*D*) Representative immunolabelings for cardiomyocytes (tropomyosin, red), fibrous tissue (fibronectin, green), and nuclei (DAPI, blue) focusing on the cardiac amputation site for untreated CTRL, T_3-treated, and perchlorate-treated tadpoles at 30 dpa. Black and white pictures showing only the tropomyosin channel are shown for each heart, facilitating myocardial wall continuity assessment. No gaps in the myocardial wall were observed for CTRL ventricles at 30 dpa, whereas the ventricles of T_3-treated and perchlorate-treated tadpoles presented an evident absence of myocardium closure, with numerous gaps observed in the myocardial wall at the amputated site for the T_3-treated heart (white arrowheads). (*E*) Immunolabeling for tropomyosin (red), fibronectin (green), and DAPI-labeled nuclei (blue) showed that compared with untreated CTRL, an invasive fibrotic zone remained detectable at the amputation site at 90 dpa in T_3-treated tadpoles and perchlorate-treated tadpoles (arrowheads indicate the amputation site). All data were obtained from more than three independent experiments. $n = 74$ (CTRL), $n = 58$ (T_3), and $n = 47$ (Perchlo) and a log-rank (Mantel–Cox) test was used to compare survival curves (ns, nonsignificant, $P > 0.05$; $^{****}P < 0.0001$). For fibrosis extent and fibronectin immunolabeling: 30 dpa, $n = 16$ (CTRL), $n = 12$ (T_3), and $n = 16$ (Perchlo); 90 dpa, $n = 11$ (CTRL), $n = 8$ (T_3), and $n = 11$ (Perchlo), and graph represented as box plot showing median with interquartile range. A nonparametric Mann–Whitney test was performed for fibrosis extent comparison (ns, nonsignificant, $P > 0.05$; $^{*}P < 0.05$; $^{**}P < 0.01$; $^{****}P < 0.0001$). (Scale bars, 100 μm in *D* and 50 μm in *E*.)

Total collagen deposition was completely eliminated at 30 dpa in the nontreated (CTRL) group, whereas it was still present at 90 dpa in T_3-treated and perchlorate-treated animals. Moreover, Col1 immunolabeling showed that its kinetics changed as a function of T_3 or perchlorate-treatment. A short transitory peak of Col1 was detected at 3 dpa in CTRL (as seen in *SI Appendix*, Fig. S3), whereas Col1 remained present at the injury site for T_3-treated and perchlorate-treated tadpoles, up to 30 dpa and 90 dpa, respectively (*SI Appendix*, Fig. S6). Interestingly, heart growth measurements (*SI Appendix*, Fig. S7) showed no significant difference in the ventricle area for both control and T_3-treated tadpoles at 90 dpa, whereas heart size was larger for perchlorate-treated tadpoles. Together, these results showed that in tadpoles both TH excess and deprivation significantly, but differentially, impact fibrotic tissue accumulation and resorption, and hence, myocardium regeneration efficiency.

TH Excess and Deprivation Before Cardiac Resection Impair Myocardial Wall Closure in Tadpoles. When we compared amputated hearts from untreated controls with T_3-treated and perchlorate-treated tadpoles, a marked difference in myocardial wall structure was observed at 30 dpa (Fig. 4*D*). The myocardial wall was closed in most of the control untreated hearts at 30 dpa (14 of 16 hearts; 87.5% closed ventricles), but presented a discontinuous wall in T_3-treated (3 of 12 hearts; 25% closed ventricles) and perchlorate-treated tadpoles (8 of 16 hearts; 50% closed ventricles), with numerous gaps observed in the majority of hearts from T_3-treated tadpoles (Fig. 4*D*). At 90 dpa, myocardial wall closure was observed in all control untreated hearts (11 of 11 hearts; 100% closed ventricles), in most of the T_3-treated tadpoles (7 of 8 hearts; 87.5% closed ventricles), but remained open for half of perchlorate-treated tadpoles (5 of 11 hearts; 45.5% closed ventricles).

TH Excess and Deprivation Significantly Modify ECM Gene Expression but Not DNA-Synthesis and Mitosis in Cardiac Tissue Postamputation. To assess TH impact on cardiomyocyte DNA synthesis after heart injury, T_3-treated, perchlorate-treated, and nontreated tadpoles were amputated, then the previously described EdU protocol was applied (Fig. 5*A*). In parallel, we also assessed TH impact on nonamputated animals. No difference in DNA synthesis was observed between the three groups after amputation, a comparable increase of $Mef2^{+}EdU^{+}$ cardiomyocyte nuclei was observed independent of TH status (Fig. 5 *B*–*E*). Similarly,

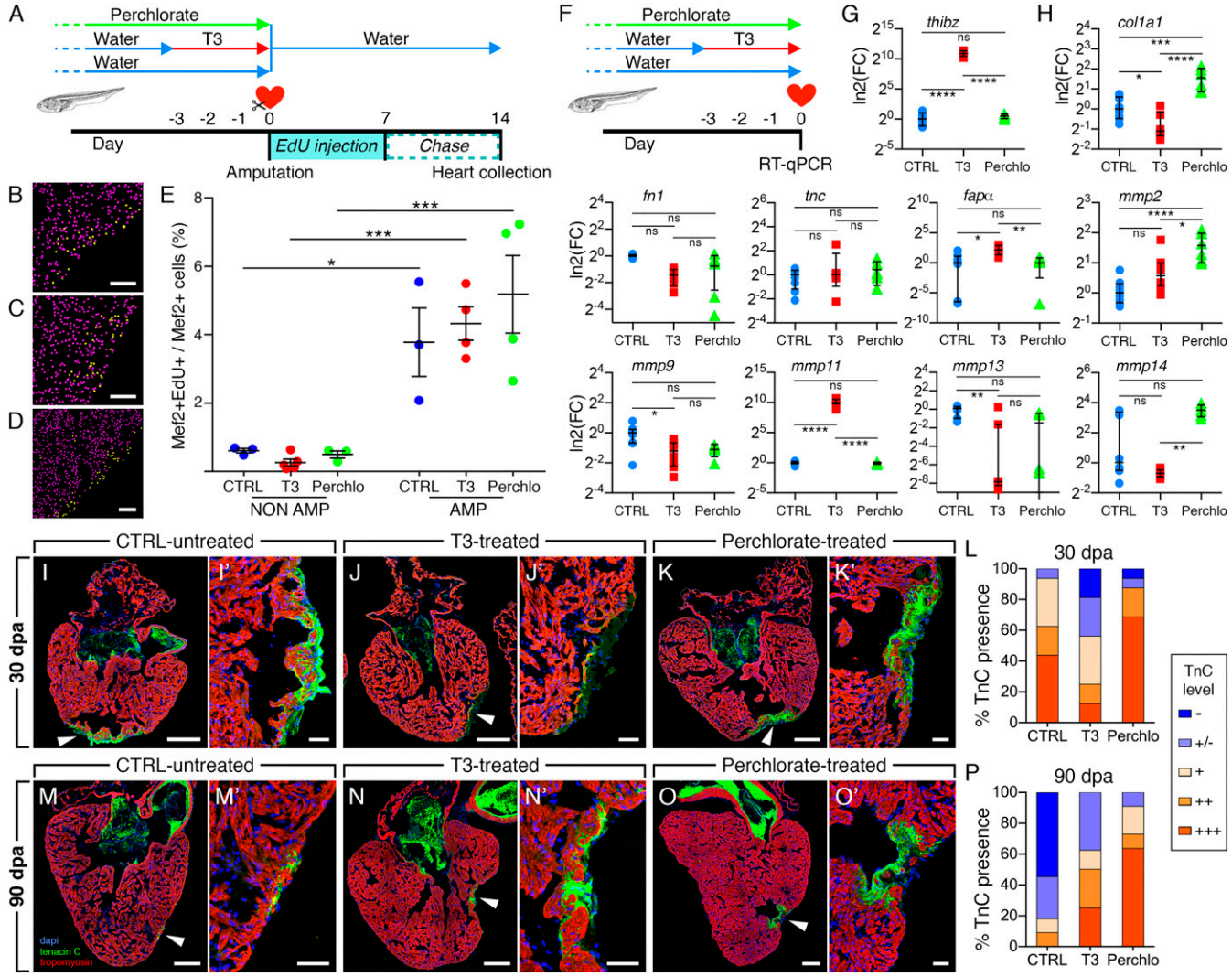

Fig. 5. Short exposure or TH deprivation prior tadpole heart amputation alters extracellular matrix components and not DNA synthesis following injury. (*A*) Control nontreated and tadpoles either T_3-treated or perchlorate-treated were amputated at day 0 and followed the same EdU protocol, as in Fig. 3. Ventricles were analyzed at 14 dpa. (*B–E*) $Mef2^+$ and $Mef2^+/EdU^+$ nuclei quantification was performed for nontreated (*B*, CTRL), T_3-treated (*C*, T_3), and perchlorate-treated (*D*, Perchlo), for nonamputated (NON AMP) and amputated (AMP) hearts, and the ratio (%) $Mef2^+EdU^+/Mef2^+$ given for each condition (*E*). Samples were obtained from three independent experiments. $n \geq 3$ per group and >3 sections were quantified per sample, and graph represented as mean with SEM. One-way ANOVA followed by Sidak's multicomparisons test was performed (*$P < 0.05$; ***$P < 0.001$). (*F*) Control untreated, T_3-treated, and perchlorate-treated tadpoles were collected at day 0 without amputation and ECM gene expression was quantified. (*G*) The TH-responsive gene *thibz* was a positive control, showing a strong induction of its expression in heart treated with T_3. (*H*) The expression of cardiac ECM genes *col1a1*, *fapα*, *mmp2*, *mmp9*, *mmp11*, *mmp13*, and *mmp14* showed a differential regulation in T_3-treated and perchlorate-treated hearts, excepted *tnc* and *fn1*, compared with control hearts. Samples were obtained from >3 independent experiments (CTRL, $n = 8$; T_3, $n = 8$; Perchlo, $n = 6$). Fold-change (FC) is shown in $\log_2$ scale, respective to CTRL. Data are represented as an aligned dot plot showing median with interquartile range. For normally distributed values (*thibz*, *fn1*, *col1a1*, *tnc*, *mmp1*, *mmp2*, *mmp11*), a one-way ANOVA followed by Sidak's multiple comparisons test was performed. For not normal distributions (*fapα*, *mmp9*, *mmp13*, *mmp14*) a nonparametric Kruskal–Wallis test followed by a Dunn's multiple comparisons test was performed. (ns, nonsignificant, $P > 0.05$; *$P < 0.05$; **$P < 0.01$; ***$P < 0.001$; ****$P < 0.0001$). (*I–P*) Impact of pharmacological treatments on TnC presence at the site of amputation at 30 dpa (*I–L*) and 90 dpa (*M–P*). Representative images are shown for CTRL untreated, T_3-treated, and perchlorate-treated tadpoles as well as a quantification of the staining intensity for TnC with the following color scheme: Absence (–, dark blue), slight staining at the ventricle surface (–/+, blue), weak (+, light orange), average (++, medium orange), and strong presence (+++, dark orange). Arrowheads (*I–O*) indicate the site of amputation, magnified in (*I′–O′*). Data were obtained from more than three independent experiments: 30 dpa, $n = 16$ (CTRL), $n = 12$ (T_3), and $n = 16$ (Perchlo); 90 dpa, $n = 11$ (CTRL), $n = 8$ (T_3), and $n = 11$ (Perchlo). [Scale bars: 100 μm (*B–D*) 200 μm (*I*, *J*, *K*, *M*, *N*, and *O*) and 50 μm (*I′*, *J′*, *K′*, *M′*, *N′*, and *O′*).]

nonamputated tadpoles displayed a weak and comparable cardiomyocyte DNA synthesis rate in the whole ventricle (Fig. 5*E*). Furthermore, examining cardiac mitotic activity in injured hearts at 3 and 7 dpa (*SI Appendix*, Fig. S8) revealed no major differences between T_3-treated, perchlorate-treated, and nontreated tadpoles. These data fit with our EdU observations (Fig. 5*E*), suggesting that modulating TH levels only weakly impacts proliferation in cardiac tissue following injury. So, the delayed cardiac regeneration observed for T_3-treated and perchlorate-treated tadpoles after heart injury (Fig. 4*C*) cannot be explained by changes in cardiomyocyte formation.

Therefore, we focused on the regulation of another important parameter in cardiac regeneration, the ECM components and remodelling enzymes. Gene expression was quantified in T_3-treated, perchlorate-treated, and nontreated tadpoles for nonamputated ventricles collected at the time when the amputation is normally performed (Fig. 5*F*). The TH-responsive gene *thibz* was used as a positive control for T_3-treatment and, as expected, was

strongly up-regulated in T_3-treated hearts, compared with nontreated and perchlorate-treated hearts (Fig. 5*G*) (19). The expression of *fibronectin 1* (*fn1*), *collagen 1* (*col1a1*), and *tenascin C* (*tnc*), genes coding for three key components of the cardiac ECM (20, 21), was quantified (Fig. 5*H*). Moreover, the expression of ECM remodelling enzymes, such as the matrix metalloproteinases *mmp2* (also known as *gelatinase A*), *mmp9* (also known as *gelatinase B*), *mmp11* (also known as *stromelysin-3*), *mmp13* (also known as *collagenase-3*), *mmp14* (also known as *membrane type 1 matrix metalloproteinase*), and *fapα* (*fibroblast activation protein α*), a family of proteinases capable of degrading various components of the ECM and involved in tissue remodelling, also regulated during *Xenopus* metamorphosis (22, 23), was analyzed (Fig. 5*H*). We observed significant alteration of *col1a1*, *mmp2*, *mmp9*, *mmp11*, *mmp13*, *mmp14*, and *fapα* expression in T_3-treated or perchlorate-treated hearts compared with nontreated hearts (Fig. 5*H*), indicating that cardiac expression of these ECM genes is sensitive to TH levels.

TH Excess or Deprivation Alter the Kinetics of Tenascin C Deposition After Tadpole Heart Resection. Given that the ECM protein tenascin C (TnC) is essential for heart regeneration (24), we next assessed the kinetics of TnC deposition in amputated hearts. We examined TnC deposition during regeneration at 30 and 90 dpa in nontreated, T_3-treated, and perchlorate-treated tadpoles (Fig. 5 *I*–*P*). At 30 dpa, T_3-treatment delayed TnC deposition at the amputation site (Fig. 5 *J* and *J′*), whereas it was strongly increased in perchlorate-treated tadpoles (Fig. 5 *K* and *K′*), compared with nontreated controls (Fig. 5 *I* and *I′*). More than 60% of control tadpoles and 90% of perchlorate-treated tadpoles had strong TnC labeling at the amputation site, whereas this was the case for only 30% of T_3-treated tadpoles (Fig. 5*L*). Conversely, at 90 dpa, TnC deposition had almost been eliminated in nontreated tadpoles (Fig. 5 *M* and *M′*), yet TnC remained strongly present in the hearts of both T_3-treated (Fig. 5 *N* and *N′*) and perchlorate-treated (Fig. 5 *O* and *O′*) animals. Less than 20% of nontreated tadpoles analyzed displayed minimal TnC presence at 90 dpa, compared with ∼60% and 70% for T_3-treated and perchlorate-treated animals, respectively (Fig. 5*P*). These results showed that TH status profoundly modifies the kinetics of TnC deposition following heart amputation. Together with the observed alteration of fibronectin and collagen deposition (Fig. 4 and *SI Appendix*, Fig. S6), and ECM gene expression modulation (Fig. 5*H*), our data suggest that modification of TH availability (excess or deprivation) significantly and differentially impacts connective tissue deposition, and thus myocardium repair after injury.

Discussion

We developed the anuran amphibian *X. laevis* as an experimental model to explore cardiac regeneration during postembryonic development and aging. We highlight stage-dependent cardiac regenerative capacities in this species, similar to that observed in mammalian models (5, 8). Hearts of prometamorphic tadpoles displayed efficient regenerative capacity (Figs. 1 and 2), as documented for zebrafish, axolotl, newt, and neonatal mammals (5, 8). This capacity is then constrained during metamorphosis, being lost in juveniles, even at 3.3 y after cardiac amputation (Fig. 2 and *SI Appendix*, Figs. S2 and S3). This finding conclusively demonstrated the loss of regenerative capacity in postmetamorphic animals. It is also consistent with our previous data showing that the adult frog heart is unable to regenerate after amputation (16), as for adult mammals (5, 8). However, our observation in juvenile and adult *X. laevis* contrasts with findings in the closely related species *Xenopus tropicalis*, which is capable of cardiac regeneration (25). A similar observation is found in teleosts, with a contrasting regenerative capacity for medaka compared with zebrafish (5, 6, 26). A common feature between nonmammalian vertebrates and young mammals that possess cardiac regenerative capacity is the absence of a sophisticated adaptive immune system compared with adult mammals (5). Notably, the anuran amphibian *Xenopus* shares many characteristics with mammals in this respect; that is, the larval immune system relies on innate immunity that is completed by an adaptive immune system in adults (27). Interestingly, the most profound immune changes occur during metamorphosis and are likely TH-dependent (27). Although both *X. laevis* and *X. tropicalis* have genes linked to antigen-specific adaptive immunity, they are often diploidized in the allotetraploid *X. laevis* (27). Consequently, as for zebrafish and medaka (26), immune system differences might account for differential cardiac regeneration capacity between *X. tropicalis* and *X. laevis* (28).

Amphibian metamorphosis is a process orchestrated by TH which drives the switch between larval and juvenile cellular phenotypes and hence life-stage transition. This event can be paralleled to mammalian postnatal development, in which comparable TH level changes, as well as remodelling events that require tissue renewal, take place (29). Our data showed that cardiac regenerative capacity in *X. laevis* is diminished during the critical period of TH-regulated metamorphosis, similar to the regenerative loss observed for numerous other tissues in this species (15). Interestingly, the temporal window during which heart regenerative capacity is lost in neonate mice (7 d after birth) (8) coincides with the first postnatal rise in TH levels (30). Analyzing the consequence of altered TH availability on cardiac regenerative capacity in efficiently regenerating tadpoles, we observed that TH excess or deprivation both negatively impacted the extent of fibrosis and myocardium repair after injury (Fig. 4). Modulation of TH status and its contrasting effects on cardiac regenerative capacity has also been previously reported in mammals, including humans. Advanced heart failure is associated with reduced levels of plasma TH (31–33). However, because circulating TH levels do not always reflect cell- and tissue-specific levels (34, 35), the role of cellular TH availability in cardiac disease as a cause or consequence of heart failure and, whether TH-induced responses are adaptive or maladaptive, remains debated (36). It could be that, as in early development or during mammalian skeletal muscle regeneration, where intracellular TH levels are finely tuned by local TH metabolism (34, 35, 37, 38), optimal cardiac regeneration requires tight control of intracellular TH, with onset and duration being critical. What is more, each different cell type contributing to the regeneration process could require specific timing of control over intracellular TH, as seen during inner ear development (39). Further analyses will be required to address the possible link between the physiological and developmental functions of TH and gene regulation exerted at the level of receptors, transporters, and deiodinases in cardiac regeneration.

The balance between ECM synthesis and degradation is crucial to tissue remodelling and regeneration following cardiac injury (20, 21). Early and transient increase of fibronectin and collagen is required for cardiac regeneration in zebrafish (40–42), yet persistence of aberrant connective tissue can lead to defects in cardiac regeneration (40) and organ failure (20). In axolotl, alteration of cardiac ECM remodelling blocks regeneration, despite the generation of novel cardiomyocytes (43). Other data in zebrafish, newt, and mouse stress the crucial role played by transient ECM deposition in the injured myocardium, which is then remodelled in coordination with effective tissue replacement (24, 43–47). Additionally, dysregulation of the ECM is often observed in human heart disease (2, 21, 48). Remarkably, ECM is a privileged TH target. TH significantly regulates a large number of ECM components and remodelling enzymes during *Xenopus* metamorphosis (22, 23, 49). Moreover, TH-induced modulations of ECM components and proteases have also been reported in mammalian hearts (50, 51). We observed that most of the ECM genes studied were differentially expressed after exposing tadpoles to TH excess or deprivation

(Fig. 5*H*). Altered expression of matrix metalloproteinases that strongly influence ECM remodelling (22, 23, 49) may explain the profound change in connective tissue deposition and dynamics observed following cardiac amputation in treated animals (Figs. 4 and 5 and *SI Appendix*, Fig. S6) and during natural metamorphosis (*SI Appendix*, Fig. S2). It is therefore tempting to hypothesize that cardiac ECM response is linked to regeneration efficiency and might be a TH-dependent limiting step. This idea is reinforced by findings in the rat, showing that *tnc* expression was down-regulated by addition of TH (52) and up-regulated in hypothyroidism (53). As elegantly demonstrated for zebrafish ECM (54), it would be interesting to see if decellularized cardiac ECM from *X. laevis* with modified TH status or from different developmental stages could initiate regenerative responses when injected into adult mammalian hearts or nonregenerative adult *Xenopus* hearts. Moreover, investigating whether TH acts directly or indirectly on heart regenerative outcome would be a promising line of inquiry. Arguing for a direct action, cardiomyocytes were shown to be TH-responsive in different species, in which a switch between fetal and adult transcriptomic programs is well documented in normal development and pathological conditions (55, 56). Given our observations relative to the alteration of ECM dynamics, others cell populations, such as cardiofibroblasts, which are also sensitive to TH action (57), may be relevant to investigate. Indirect mechanisms could relate to immune cell activity, also known to be regulated by TH (58, 59). Interestingly, macrophages possess ECM remodeling activity via the expression of mmps (60), and are involved in the development of fibrosis in skeletal muscle (61) and necessary for cardiac regeneration through fibroblast activation in salamander (43).

In summary, our data provide a perspective on the enigmatic loss of cardiac regenerative capacity during vertebrate development, and highlight an unexplored role of TH availability that might be involved in this process. Given that heart regeneration is lost in a physiologically similar period in mice and *X. laevis*, comparative analysis of these models should increase understanding of how TH can modulate cardiac regenerative outcome. Therefore, we propose *X. laevis* as an excellent alternative model, complementary to the postnatal mouse, to decipher the developmental switches underlying diminished cardiac regenerative ability.

Materials and Methods

Animals and Ethics Statement. The care and treatment of animals were in accordance with Institutional and National Guidelines (Commission de Génie Génétique, "Direction Départementale des Services Vétérinaires," European Union Directive 2010/63/EU, agreement decision no. C75-05–01-2 for the European Convention for vertebrate animals used for experimental and other scientific purposes). All protocols used in this study were approved under the reference number 68–037 by the Ethical Committee of the National Museum of Natural History (Paris). Animals were purchased from the *Xenopus* Biological Resource Centre (Rennes, France). Studies involved *X. laevis* NF57 tadpoles to adult frogs staged using Nieuwkoop and Faber (NF) nomenclature (62); representative stage pictures were sourced from the *Xenopus* online resources website (www.xenbase.org/entry/, RRID:SCR_003280). Animals were housed in a facility with 12:12-h light:dark cycles, 18–20 °C ambient temperature, dechlorinated and filtered water, and a commercial diet (Nettle powder or TetraRubin granules depending on age). For adapting thyroid status, tadpoles were either treated with TH T_3 (10^{-10} M or 5×10^{-9} M for gene expression; in tank water, renewed daily) for 3 d for an increased TH availability (TH excess), or raised in dechlorinated and filtered water with added sodium perchlorate for at least 2 mo (0.33 g/L, renewed twice a week) to block TH production (TH deprivation). Perchlorate prevents iodine uptake (63), which inhibits TH production in the thyroid gland, through inhibition of key proteins in the TH synthesis pathway, including the sodium-iodide symporter and thyroperoxidase (64–66), thus creating a hypothyroid state (reduced TH state).

Cardiac Resection Method. Animals were anesthetized in buffered 0.1% tricaine methanesulfonate (Ethyl 3-aminobenzoate methanesulfonate; Sigma) until the righting reflex was lost. After rinsing in dechlorinated water, animals were transferred to a moist gauze-covered mold. The skin and body wall covering the pericardium were opened using surgical forceps for NF57 to NF66 animals and microscissors for froglets and 6-mo-old juveniles. The pericardium was then pinched open revealing the heart. Stopping at this step provided sham-operated samples (meaning an operation but no resection, SHAM). A resection was performed using microscissors by removing a piece of tissue from the ventricle apex (AMP). Size of the amputation for NF57 to froglet stages represented ∼10–15% of the ventricle, and ∼8% for juvenile. Nonoperated animals were only anesthetized and used as controls (CTRL) for comparison between sham-operated and amputated samples.

Sample Preparation. Before being processed for histological and immunohistochemical analyses, hearts were collected, paraformaldehyde-fixed [4% in PBS (Sigma)] for 7 h (NF57-froglet) or 20 h (juvenile) at 4 °C, equilibrated overnight in 15% sucrose in PBS, mounted in FSC22 frozen section compound (Sigma). Sagittal sections were performed at −24 °C using a cryostat (Leica CM30050S) at a thickness of 8 μm (Figs. 1, 2, 4, and 5 *I–O* and *SI Appendix*, Figs. S1–S3, S6, and S8) or 12 μm (Figs. 3 and 5 *B–D* and *SI Appendix*, Fig. S5).

Immunohistochemistry. Sagittal heart sections were preincubated with 1% SDS (Sigma) in PBS for 5 min to allow for antigen unmasking. Then immunodetection was carried out as previously described (16), using the following antibodies: mouse anticardiac tropomyosin (#CH1; 1:1,000; DSHB), rabbit antifibronectin1 (#F3648; 1:500; Sigma), rabbit antitenascin C (#AB19013; 1:500; Merck), rabbit anticollagen1 (#2150–1410; 1:500; Bio-Rad), rabbit antimyocyte enhancer factor-2 antibody (#C21; 1:500; Santa Cruz Biotechnology), mouse antiphospho-histone H3 antibody (#05–806; 1:300; Millipore), and the appropriate fluorescent secondary antibodies (1:1,500; Invitrogen). EdU labeling was carried out using the Click-iT Plus EdU Alexa Fluor 594 Imaging Kit and following manufacturer recommendations (C10639; Life Technologies), preceded by immunodetection with the rabbit anti-Mef2 antibody. All sections were counterstained with DAPI (Molecular Probes) for 10 min, followed by mounting with Prolong diamond antifade reagent (Thermofisher) and imaged with a confocal microscope (Leica TCS SP5) or a fluorescence microscope (Leica DM5500B microscope and DFC450C camera with Prior Lumen200 light source). All fluorescent images were posttreated in Photoshop (Adobe), and merged using NIH ImageJ software.

Picrosirius Red Labeling. As previously described (16), sagittal heart sections were postfixed for 30 min in formalin 10% (Sigma), followed by overnight fixation in Bouin's solution (Sigma), and then extensively washed with tap water. Sections were incubated for 1 h in Picrosirius red (PSR) solution: 0.1% direct red 80 (Sigma) and 0.1% fast green FCF (Sigma) in saturated aqueous picric acid (1.2% picric acid in water; Sigma). Sections were quickly washed 10 times in distilled water, twice in 70% ethanol, then in 100% ethanol (2 × 15 min), and finally in Safesolv solution (Q Path, VWR International; 2 × 15 min), before being mounted in safemount medium (Q Path, VWR International). The slides were then imaged using a stereomicroscope (Leica MZ16F with QImaging Retiga camera) or a light microscope (Leica DM5500B and DFC450C camera).

Acid Fuchsin Orange-G Labeling. Sagittal heart sections were postfixed in 10% formalin (Sigma) for 30 min, followed by overnight fixation in Bouin's solution (Sigma), and then extensively washed with tap water. Acid Fuchsin Orange-G staining was performed as previously described (17, 40). Sections were incubated in Safesolv solution (Q Path, VWR International; 2 × 15 min), before being mounted in safemount medium (Q Path, VWR International). The slides were then imaged using a stereomicroscope (Leica MZ16F with QImaging Retiga camera) or a light microscope (Leica DM5500B and DFC450C camera).

EdU Proliferation Protocol. Following operation, daily intraperitoneal EdU injections were performed for 1 wk (pulse) (30 μg per injection for NF57 tadpoles, diluted in 6 μL PBS and 300 μg per injection for 6-mo-old juveniles, diluted in 200 μL PBS), followed by a 1-wk chase, before animals were killed at 14 dpa and heart analyzed by immunolabeling. The same EdU injection procedure was used for control and sham-operated animals.

Image Analysis. Following confocal image acquisition, a *z*-stack image for each heart section was posttreated using NIH ImageJ software to remove the atria and restrict the stack to the ventricle area, which was then transferred to IMARIS software v7.4.2 (Bitplane). Using the spot function, the total number of $Mef2^+$ cells from the whole ventricle stack was quantified, and from those, the number of $Mef2^+$ cells colabeled with EdU^+ was counted. The

ratio ($Mef2^+EdU^+/Mef2^+$) provides the percentage of new cardiomyocytes formed at 14 dpa.

Fibrosis Extent Analysis. Heart samples collected at 30 and 90 dpa were fully sectioned. For each sample, one section in every eight was analyzed to obtain a serial representation of the whole ventricle. After CH1/Fn1 immunolabeling, fibrosis extent was assessed by monitoring the presence or absence of fibronectin and a "fibrotic severity" index for each heart was assigned as follows: [0] no fibrotic connective tissue at the site of injury, [1] slight presence of fibrotic connective tissue at the site of injury, [2] large deposition of fibrotic connective tissue at the site of injury, and [3] intense and invasive deposition of connective tissue at the site of injury, with a discontinuous underlying myocardium wall showing gaps. To calculate fibrosis extent, the index was then multiplied by the number of sections that displayed a mark of amputation ($N^{amp\text{-}mark}$), and divided by the total number of sections for that sample (N^{total}). Therefore, we applied the following formula: (fibrotic severity index) × ($N^{amp\text{-}mark}$)/(N^{total}). A nonparametric Mann–Whitney test was used for fibrosis extent comparison.

Survival Curve Analysis. Tadpole survival is represented as a Kaplan–Meier survival plot and the log-rank (Mantel–Cox) test was used to compare survival curves (Prism7.0, GraphPad).

RNA Extraction. Tadpole hearts were cleaned from atrium and arterial bulb, then ventricles were cut in half, thoroughly washed in PBS to eliminate blood, and snap-frozen (individually) in liquid nitrogen. Total RNAs were extracted using RNAqueous Micro Kit RNA isolation from Microscale and LCM Sample (Ambion). Total RNAs were quantified and quality controlled using Qubit (Thermo Fisher Scientific) and 2100 Bioanalyser (Agilent Technologies), respectively. Samples with RNA integrity (RIN) of ≥7 (average RIN 8.6) were retained for qPCR analyses.

Standard Real-Time Quantitative PCR. For real-time qPCR, RNA samples from nontreated controls, T_3-treated, and perchlorate-treated animals were reverse transcribed using High-Capacity cDNA Reverse Transcription kit (Applied Biosystems) using a MyCyclerTM (Bio-Rad), following the manufacturer's recommendations. Real-time qPCR reactions were performed in duplicate for each sample using Power SYBR master mix on a QuantStudio 6 Flex Real-Time PCR System (Applied Biosystems), following the manufacturer's recommendations. Primer sequences used for *thibz*, *fn1*, *col1a1*, and *tnc* are detailed in *SI Appendix*, Table S1, or already published for *mmp2*, *mmp9*, *mmp11*, *mmp13*, *mmp14*, and *fapα* (22, 23). Ct data were collected using ExpressionSuite Software (Applied Biosystems) and analyzed using Excel (Microsoft). The Cts for each technical duplicate were averaged and normalized (ΔCt) against the geometric mean of the two reference genes *smarcd1* and *smn2* (16). Variations of expression were quantified by the ΔΔCts Livak method (67), using the control condition as references for each experimental time-point and fold-changes were computed as $2^{-\Delta\Delta Ct}$. Outliers were identified and eliminated with ROUT test method (Q = 1%), before performing statistical analysis on ΔCts values (GraphPad Prism 7.0).

Data and Materials Availability. All data used in the paper are present in the main text and *SI Appendix*.

ACKNOWLEDGMENTS. We thank Gérard Bénisti, Philippe Durand, and Jean-Paul Chaumeil for outstanding animal care; Jean-Baptiste Fini for constructive manuscript feedback; Vincent Contremoulins for IMARIS guideance; and the ImagoSeine facility, member of the France BioImaging infrastructure supported by the French National Research Agency (ANR-10-INBS-04, "Investments of the future"). The research leading to these results has received funding from European Union Grant Crescendo and the French PNR-PE Program; Watchfrog S.A. under CIFRE Convention 216/2011 PhD fellowship (to C.J.V.); and the People Programme (Marie Curie Actions) of the European Union's Seventh Framework Programme FP7-2013 under Reemployment and Eligibility Assessment Grant 607142, DevCom PhD fellowship (to L.N.M.).

1. World Health Organisation (2018) The top 10 causes of death: Fact sheet. Available at https://www.who.int/en/news-room/fact-sheets/detail/the-top-10-causes-of-death. Accessed February 1, 2019.
2. Tzahor E, Poss KD (2017) Cardiac regeneration strategies: Staying young at heart. *Science* 356:1035–1039.
3. Laflamme MA, Murry CE (2011) Heart regeneration. *Nature* 473:326–335.
4. Gamba L, Harrison M, Lien CL (2014) Cardiac regeneration in model organisms. *Curr Treat Options Cardiovasc Med* 16:288.
5. Vivien CJ, Hudson JE, Porrello ER (2016) Evolution, comparative biology and ontogeny of vertebrate heart regeneration. *NPJ Regen Med* 1:16012.
6. Ito K, et al. (2014) Differential reparative phenotypes between zebrafish and medaka after cardiac injury. *Dev Dyn* 243:1106–1115.
7. Blau HM, Pomerantz JH (2011) Re"evolutionary" regenerative medicine. *JAMA* 305: 87–88.
8. Porrello ER, et al. (2011) Transient regenerative potential of the neonatal mouse heart. *Science* 331:1078–1080.
9. Zogbi C, et al. (2014) Early postnatal rat ventricle resection leads to long-term preserved cardiac function despite tissue hypoperfusion. *Physiol Rep* 2:e12115.
10. Herdrich BJ, et al. (2010) Regenerative healing following foetal myocardial infarction. *Eur J Cardiothorac Surg* 38:691–698.
11. Ye L, et al. (2018) Early regenerative capacity in the porcine heart. *Circulation* 138: 2798–2808.
12. Malyshev II (1975) The recovery process in the fetal rabbit myocardium following mechanical trauma. *Biull Eksp Biol Med* 80:111–113.
13. Malyshev II (1977) Regeneration of the myocardium of fetuses and newborn rabbits. *Arkh Patol* 39:53–58.
14. Haubner BJ, et al. (2016) Functional recovery of a human neonatal heart after severe myocardial infarction. *Circ Res* 118:216–221.
15. Beck CW, Izpisúa Belmonte JC, Christen B (2009) Beyond early development: *Xenopus* as an emerging model for the study of regenerative mechanisms. *Dev Dyn* 238: 1226–1248.
16. Marshall L, et al. (2017) Persistent fibrosis, hypertrophy and sarcomere disorganisation after endoscopy-guided heart resection in adult *Xenopus*. *PLoS One* 12: e0173418.
17. Poss KD, Wilson LG, Keating MT (2002) Heart regeneration in zebrafish. *Science* 298: 2188–2190.
18. Brown DD, Cai L (2007) Amphibian metamorphosis. *Dev Biol* 306:20–33.
19. Furlow JD, Brown DD (1999) In vitro and in vivo analysis of the regulation of a transcription factor gene by thyroid hormone during *Xenopus laevis* metamorphosis. *Mol Endocrinol* 13:2076–2089.
20. Bonnans C, Chou J, Werb Z (2014) Remodelling the extracellular matrix in development and disease. *Nat Rev Mol Cell Biol* 15:786–801.
21. Frangogiannis NG (2017) The extracellular matrix in myocardial injury, repair, and remodeling. *J Clin Invest* 127:1600–1612.
22. Fujimoto K, Nakajima K, Yaoita Y (2007) Expression of matrix metalloproteinase genes in regressing or remodeling organs during amphibian metamorphosis. *Dev Growth Differ* 49:131–143.
23. Naitoh H, et al. (2017) Upregulation of matrix metalloproteinase triggers transdifferentiation of retinal pigmented epithelial cells in *Xenopus laevis*: A link between inflammatory response and regeneration. *Dev Neurobiol* 77:1086–1100.
24. Mercer SE, Odelberg SJ, Simon HG (2013) A dynamic spatiotemporal extracellular matrix facilitates epicardial-mediated vertebrate heart regeneration. *Dev Biol* 382: 457–469.
25. Liao S, et al. (2017) Heart regeneration in adult *Xenopus tropicalis* after apical resection. *Cell Biosci* 7:70.
26. Lai SL, et al. (2017) Reciprocal analyses in zebrafish and medaka reveal that harnessing the immune response promotes cardiac regeneration. *eLife* 6:e25605.
27. Robert J, Ohta Y (2009) Comparative and developmental study of the immune system in *Xenopus*. *Dev Dyn* 238:1249–1270.
28. Marshall L, Girardot F, Demeneix BA, Coen L (2018) Is adult cardiac regeneration absent in *Xenopus laevis* yet present in *Xenopus tropicalis*? *Cell Biosci* 8:31.
29. Paris M, Laudet V (2008) The history of a developmental stage: Metamorphosis in chordates. *Genesis* 46:657–672.
30. Hadj-Sahraoui N, Seugnet I, Ghorbel MT, Demeneix B (2000) Hypothyroidism prolongs mitotic activity in the post-natal mouse brain. *Neurosci Lett* 280:79–82.
31. Janssen R, Muller A, Simonides WS (2017) Cardiac thyroid hormone metabolism and heart failure. *Eur Thyroid J* 6:130–137.
32. Gerdes AM, Iervasi G (2010) Thyroid replacement therapy and heart failure. *Circulation* 122:385–393.
33. de Vries EM, Fliers E, Boelen A (2015) The molecular basis of the non-thyroidal illness syndrome. *J Endocrinol* 225:R67–R81.
34. Dentice M, Marsili A, Zavacki A, Larsen PR, Salvatore D (2013) The deiodinases and the control of intracellular thyroid hormone signaling during cellular differentiation. *Biochim Biophys Acta* 1830:3937–3945.
35. Bianco AC, Kim BW (2006) Deiodinases: Implications of the local control of thyroid hormone action. *J Clin Invest* 116:2571–2579.
36. Pol CJ, Muller A, Simonides WS (2010) Cardiomyocyte-specific inactivation of thyroid hormone in pathologic ventricular hypertrophy: An adaptative response or part of the problem? *Heart Fail Rev* 15:133–142.
37. Salvatore D, Simonides WS, Dentice M, Zavacki AM, Larsen PR (2014) Thyroid hormones and skeletal muscle—New insights and potential implications. *Nat Rev Endocrinol* 10:206–214.
38. Ambrosio R, De Stefano MA, Di Girolamo D, Salvatore D (2017) Thyroid hormone signaling and deiodinase actions in muscle stem/progenitor cells. *Mol Cell Endocrinol* 459:79–83.
39. Ng L, et al. (2004) Hearing loss and retarded cochlear development in mice lacking type 2 iodothyronine deiodinase. *Proc Natl Acad Sci USA* 101:3474–3479.
40. Chablais F, Jazwinska A (2012) The regenerative capacity of the zebrafish heart is dependent on TGFβ signaling. *Development* 139:1921–1930.

41. Wang J, Karra R, Dickson AL, Poss KD (2013) Fibronectin is deposited by injury-activated epicardial cells and is necessary for zebrafish heart regeneration. *Dev Biol* 382:427–435.
42. Sallin P, Jaźwińska A (2016) Acute stress is detrimental to heart regeneration in zebrafish. *Open Biol* 6:160012.
43. Godwin JW, Debuque R, Salimova E, Rosenthal NA (2017) Heart regeneration in the salamander relies on macrophage-mediated control of fibroblast activation and the extracellular landscape. *NPJ Regen Med* 2:22.
44. Bassat E, et al. (2017) The extracellular matrix protein agrin promotes heart regeneration in mice. *Nature* 547:179–184.
45. Franz M, et al. (2010) Changes in extra cellular matrix remodelling and re-expression of fibronectin and tenascin-C splicing variants in human myocardial tissue of the right atrial auricle: Implications for a targeted therapy of cardiovascular diseases using human SIP format antibodies. *J Mol Histol* 41:39–50.
46. Yokokawa T, et al. (2016) Significance of myocardial tenascin-C expression in left ventricular remodelling and long-term outcome in patients with dilated cardiomyopathy. *Eur J Heart Fail* 18:375–385.
47. Shimojo N, et al. (2015) Tenascin-C may accelerate cardiac fibrosis by activating macrophages via the integrin αVβ3/nuclear factor-κB/interleukin-6 axis. *Hypertension* 66:757–766.
48. Xin M, Olson EN, Bassel-Duby R (2013) Mending broken hearts: Cardiac development as a basis for adult heart regeneration and repair. *Nat Rev Mol Cell Biol* 14:529–541.
49. Shi YB, Fu L, Hasebe T, Ishizuya-Oka A (2007) Regulation of extracellular matrix remodeling and cell fate determination by matrix metalloproteinase stromelysin-3 during thyroid hormone-dependent post-embryonic development. *Pharmacol Ther* 116:391–400.
50. Jabbar A, et al. (2017) Thyroid hormones and cardiovascular disease. *Nat Rev Cardiol* 14:39–55.
51. Pingitore A, et al. (2016) Cardioprotection and thyroid hormones. *Heart Fail Rev* 21: 391–399.
52. González-Sancho JM, Alvarez-Dolado M, Caelles C, Muñoz A (1999) Inhibition of tenascin-C expression in mammary epithelial cells by thyroid hormone. *Mol Carcinog* 24:99–107.
53. Alvarez-Dolado M, González-Sancho JM, Bernal J, Muñoz A (1998) Developmental expression of the tenascin-C is altered by hypothyroidism in the rat brain. *Neuroscience* 84:309–322.
54. Chen WC, et al. (2016) Decellularized zebrafish cardiac extracellular matrix induces mammalian heart regeneration. *Sci Adv* 2:e1600844.
55. Chattergoon NN, et al. (2012) Thyroid hormone drives fetal cardiomyocyte maturation. *FASEB J* 26:397–408.
56. Zhang D, et al. (2017) microRNA and thyroid hormone signaling in cardiac and skeletal muscle. *Cell Biosci* 7:14.
57. Yao J, Eghbali M (1992) Decreased collagen gene expression and absence of fibrosis in thyroid hormone-induced myocardial hypertrophy. Response of cardiac fibroblasts to thyroid hormone in vitro. *Circ Res* 71:831–839.
58. Jara EL, et al. (2017) Modulating the function of the immune system by thyroid hormones and thyrotropin. *Immunol Lett* 184:76–83.
59. De Vito P, et al. (2011) Thyroid hormones as modulators of immune activities at the cellular level. *Thyroid* 21:879–890.
60. Goetzl EJ, Banda MJ, Leppert D (1996) Matrix metalloproteinases in immunity. *J Immunol* 156:1–4.
61. Alameddine HS, Morgan JE (2016) Matrix metalloproteinases and tissue inhibitor of metalloproteinases in inflammation and fibrosis of skeletal muscles. *J Neuromuscul Dis* 3:455–473.
62. Nieuwkoop PD, Faber J (1994) *Normal Table of Xenopus laevis (Daudin): A Systematical and Chronological Survey of the Development from the Fertilized Egg Till the End of Metamorphosis* (Garland, New York).
63. Leung AM, Pearce EN, Braverman LE (2010) Perchlorate, iodine and the thyroid. *Best Pract Res Clin Endocrinol Metab* 24:133–141.
64. Tietge JE, et al. (2005) Metamorphic inhibition of *Xenopus laevis* by sodium perchlorate: Effects on development and thyroid histology. *Environ Toxicol Chem* 24: 926–933.
65. Tietge JE, et al. (2010) Early temporal effects of three thyroid hormone synthesis inhibitors in *Xenopus laevis*. *Aquat Toxicol* 98:44–50.
66. Hornung MW, et al. (2010) Inhibition of thyroid hormone release from cultured amphibian thyroid glands by methimazole, 6-propylthiouracil, and perchlorate. *Toxicol Sci* 118:42–51.
67. Livak KJ, Schmittgen TD (2001) Analysis of relative gene expression data using real-time quantitative PCR and the 2(-Delta Delta C(T)) method. *Methods* 25:402–408.